Divergent historical GPP trends among state-of-the-art multi-model simulations and satellite-based products

Ruqi Yang[1,2], Jun Wang[3,4*], Ning Zeng[1,5], Stephen Sitch[6], Wenhan Tang[1,2], Matthew Joseph McGrath[7], Qixiang Cai[1], Di Liu[1], Danica Lombardozzi[8], Hanqin Tian[9], Atul K Jain[10], Pengfei Han[1,11]

[1]State Key Laboratory of Numerical Modeling for Atmospheric Sciences and Geophysical Fluid Dynamics, Institute of Atmospheric Physics, Chinese Academy of Sciences, Beijing, China
[2]College of Earth and Planetary Sciences, University of Chinese Academy of Sciences, Beijing 100049, China
[3]Jiangsu Provincial Key Laboratory of Geographic Information Science and Technology, International Institute for Earth System Science, Nanjing University, Nanjing, Jiangsu 210023, China
[4]Frontiers Science Center for Critical Earth Material Cycling, Nanjing University, Nanjing, Jiangsu 210023, China
[5]Department of Atmospheric and Oceanic Science, and Earth System Science Interdisciplinary Center, University of Maryland, College Park, Maryland, USA
[6]College of Life and Environmental Sciences, University of Exeter, UK.
[7]Laboratoire des Sciences du Climat et de l'Environnement/Institut Pierre Simon Laplace, Commissariat à l'Énergie, Atomique et aux Énergies Alternatives–CNRS–Université de Versailles Saint-Quentin, Université Paris-Saclay, F-91191 Gif-sur-Yvette, France
[8]National Center for Atmospheric Research, Climate and Global Dynamics Laboratory, Boulder, CO, USA
[9]International Center for Climate and Global Change Research, School of Forestry and Wildlife Sciences, Auburn University, Auburn, AL 36849, USA.
[10]Department of Atmospheric Science, University of Illinois, Urbana, IL 61801, USA
[11]Carbon Neutrality Research Center, Institute of Atmospheric Physics, Chinese Academy of Sciences, Beijing, China

Correspondence to: Jun Wang (wangjun@nju.edu.cn)

Abstract. Understanding historical changes in gross primary productivity (GPP) is essential for better predicting the future global carbon cycle. However, the historical trends of terrestrial GPP, owing to the CO_2 fertilization effect, climate, and land-use change, remain largely uncertain. Using long-term satellite-based near-infrared radiance of vegetation (NIRv), a proxy for GPP, and multiple GPP datasets derived from satellite-based products, Dynamic Global Vegetation Model (DGVM) simulations, and an upscaled product from eddy covariance (EC) measurements, here we comprehensively investigated their trends and analyzed the causes for any discrepancies during 1982–2015. Although spatial patterns of climatological annual GPP from all products and NIRv are highly correlated ($r > 0.84$), the spatial correlation coefficients of trends between DGVM GPP and NIRv significantly decreased (with the ensemble mean of $r = 0.49$) and even the spatial correlation coefficients of trends between other GPP products and NIRv became negative. By separating the global land into the tropics plus extra-tropical southern hemisphere (Trop+SH) and extra-tropical northern hemisphere (NH), we found that, during 1982–2015, simulated GPP from most of the models showed a stronger increasing trend over Trop+SH than NH. In contrast, the satellite-based GPP products indicated a substantial increase over NH. Mechanistically, model sensitivity experiments indicated that the increase of annual global total GPP was dominated by the CO_2 fertilization effect (83.9% contribution), however, with the largest uncertainty in magnitude in individual simulations among the three drivers of CO_2 fertilization, climate, and land-use

删除了: [4]Jiangsu Provincial Key Laboratory of Geographic Information Science and Technology, Key Laboratory for Land Satellite Remote Sensing Applications of Ministry of Natural Resources, School of Geography and Ocean Science, Nanjing University, Nanjing, Jiangsu 210023, China

删除了: ,

删除了: and machine learning techniques

change. Interestingly, the spatial distribution of inter-model spreads of GPP trends resulted mainly from climate and land-use change rather than CO_2 fertilization effect. After 2000, trends from satellite-based GPP products were different from the full time-series, suggesting weakened rising trends over NH and even significantly decreasing trends over Trop+SH, while the trends from DGVMs and NIRv kept increasing. The inconsistencies of GPP trends are very likely caused by the contrasting performances between satellite-derived and DGVM simulated vegetation structure parameter (leaf area index, LAI). Therefore, the uncertainty in satellite-based GPP products induced by highly uncertain LAI data in the tropics undermines their roles in assessing the performance of DGVM simulations and understanding the changes of global carbon sinks. The higher consistency between DGVM GPP and NIRv suggests that the trends from DGVM ensemble might even have better performance than satellite-based GPP products.

删除了: Mechanistically, model sensitivity experiments indicated that the increase of annual GPP was dominated by the CO_2 fertilization effect (Global: 83.9%), albeit a large uncertainty in magnitude among individual simulations. However, the spatial distribution of inter-model spreads of GPP trends resulted mainly from climate and land-use change rather than CO_2 fertilization effect

设置了格式: 下标

删除了: T

删除了: after 2000

删除了: showing that satellite-based GPP products

删除了: ed

1 Introduction

The gross primary productivity (GPP) is the largest carbon flux in the terrestrial carbon cycle. Quantifying terrestrial GPP and understanding its variations are vital in the global and regional carbon cycle (Ryu et al., 2019). To date, there are multiple global GPP products, mainly including the up-scaled products from the eddy covariance (EC) flux data by machine learning techniques (Beer et al., 2010; Jung et al., 2020), satellite-based estimates by light-use efficiency (LUE) model (Running et al., 2004; Yuan et al., 2010; Joiner et al., 2018; Zheng et al., 2020), and simulations by the state-of-the-art Dynamic Global Vegetation Models (DGVMs) (Huntzinger et al., 2013; Sitch et al., 2015).

删除了: and the ecosystem respiration (ER) dominate carbon fluxes from terrestrial ecosystems. Therefore,

删除了: q

删除了: global

删除了: is

删除了: essential to understanding

The machine learning FLUXCOM GPP products based on the global FLUXNET network, remote sensing, and meteorological input (Jung et al., 2020; Pastorello et al., 2020) are widely used in terrestrial carbon cycle studies. Taking FLUXCOM GPP as a benchmark, researches have explored the interannual variation, seasonal cycle, and climatology pattern of global and regional GPP (Chen et al., 2017; Jia et al., 2020; Zhang and Ye, 2021). However, due to the lack of the CO_2 fertilization effect, the performance of this product on the long-term GPP trend is not realistic (Jung et al., 2020). Based on the LUE principle and derived from the Advanced Very High-Resolution Radiometer (AVHRR) and the Moderate Resolution Imaging Spectroradiometer (MODIS) datasets, the satellite-based GPP estimates include MOD17, GLASS, GIMMS, FluxSat, WECANN, and revised EC_LUE GPP product (Running et al., 2004; Yuan et al., 2007; Smith et al., 2016; Alemohammad et al., 2017; Joiner et al., 2018; Zheng et al., 2020). These GPP products capture the seasonal variation, spatial distribution, and interannual variation to a large extent (Wang et al., 2014), but do not always account for the CO_2 fertilization effect (O'sullivan et al., 2020). For DGVM simulations, different forcing datasets, parameterizations, and processes considered can make the surprising differences in model representation of responses of photosynthesis to CO_2 concentration, soil moisture, temperature, and water vapor deficit (Rogers, 2014; Rogers et al., 2017; Ito et al., 2017; M. Wang et al., 2021). These differences caused large inter-model spreads in GPP simulations (Ito et al., 2017). Hence, many efforts have been made to constrain the global

删除了: has

GPP magnitude based on the satellite observations like solar-induced chlorophyll fluorescence (SIF) (Macbean et al., 2018; Bacour et al., 2019; Norton et al., 2019; J. Wang et al., 2021a).

The application of satellite-derived GPP proxy datasets provides a breakthrough for estimating global GPP (Running et al., 2004; Badgley et al., 2019; Piao et al., 2020). Many GPP proxy indices, such as normalized difference vegetation index (NDVI), enhanced vegetation index (EVI), and SIF, have been widely used to estimate the global GPP (Frankenberg et al., 2011; Guanter et al., 2014). However, each of them has its shortcomings. For example, NDVI can be saturated in tropical regions, demonstrating its nonlinear relationship with GPP (Badgley et al., 2017; Badgley et al., 2019; Camps-Valls et al., 2021). The EVI index improves the NDVI algorithm, but this index has not entirely solved the saturation problem (Huete et al., 2002). Without dealing with the problem of distinguishing whether the signal comes from the plant or other interference factors, satellite retrieval of SIF measures the light emitted by chlorophyll in leaves and can be used as a robust proxy of GPP (Frankenberg et al., 2011; Mohammed et al., 2019). However, the time range of global SIF products is short, with direct observations only available from 2007. Representing the proportion of reflected near-infrared radiation attributable to vegetation, long-term satellite-derived near-infrared radiance of vegetation (NIRv) is a relatively recent GPP proxy (Badgley et al., 2017). Compared to NDVI and EVI, the saturation problem of NIRv and GPP in the tropical region is weakened because the mixed effects of background brightness, leaf area, and the distribution of canopy photosynthetic capacity with depth are largely eliminated. Since NIRv can be directly obtained from observational datasets of the AVHRR sensors, it can be derived from 1982 to the present. Moreover, previous studies have shown that NIRv and SIF are closely related and indicated that NIRv could well represent changes in GPP (Badgley et al., 2017; Badgley et al., 2019; Camps-Valls et al., 2021; S. Wang et al., 2021).

Although there have been a lot of studies focusing on extreme anomalies, the seasonal cycle, interannual variation, and the climatological pattern of global and regional GPP based on the multiple GPP products and proxy indices (Chen et al., 2017; Madani et al., 2020; J. Wang et al., 2021b), few efforts have been devoted to evaluate the long-term GPP trends across different GPP sources and to analyze the causes of uncertainties. This study will comprehensively investigate historical GPP trends during 1982−2015, based on the satellite-derived GPP proxy (NIRv), simulations from process-based models, machine-learning products, satellite-based estimates, and site-level observations. Hereinafter, section 2 describes the datasets and statistical methods used. The comparison of GPP trends among GPP proxy, DGVM simulations, and satellite-based GPP products is in section 3.1. The mechanisms of the trend attributions are explored in section 3.2. The uncertainties in GPP trends are discussed in section 3.3. At last, the main conclusions of the results are summarized in section 4.

删除了: Hashimoto et al., 2013;
删除了: L
删除了: based
删除了: NIRv
删除了: of
删除了: were
删除了: c
删除了: s
删除了: TRENDYv6 multi-model simulations
删除了: S
删除了: proposed and explained
删除了: discussions about the
删除了: included
删除了: Finally
删除了: ↵

2 Datasets and methods

2.1 TRENDYv6 multi-model simulated GPP

We used the model simulation results conducted under the auspices of the "Trends and drivers of the regional scale sources and sinks of carbon dioxide" (TRENDY) Project (Sitch et al., 2015). We used 10 DGVMs in the TRENDYv6 project for the period of 1982-2015, including CABLE (Haverd et al., 2018), CLASS-CTEM (Melton and Arora, 2016), CLM4.5 (Oleson et al., 2010), DLEM (Tian et al., 2015), ISAM (Jain et al., 2013), OCN (Zaehle et al., 2010), ORCHIDEE-MICT (Guimberteau et al., 2018), ORCHIDEE (Krinner et al., 2005), VEGAS (Zeng et al., 2005), and VISIT (Kato et al., 2013). There is a suite of experimental protocols in the TRENDY project, and we here explored GPP trends and their mechanisms using the GPP outputs from three simulations. In detail, DGVMs were run under the varying CO_2 concentration, and constant climate conditions and land-use change in S1; the varying CO_2 concentration and climate conditions, with constant land-use change in S2; the varying CO_2 concentration, climate conditions, and land-use change in S3. Hence, the S1 scenario represents the impact of the CO_2 fertilization effect. The contributions of climate change and land-use change (hereafter "LUC") are calculated through the differences between S2 and S1, S3 and S2, respectively. These modelling details are listed in Table 1.

In sections 3.2 and 3.3.1, we calculated the ensemble mean of the 7 model simulations, which included all scenarios as the DGVM ensemble GPP and calculated their standard deviation to represent inter-model spread across these models. In other sections which only need results from S3, we used the ensemble mean simulations from 10 models.

Table 1. Information of TRENDYv6 models used in this study. S1 represents the impact of the CO_2 fertilization effect, S2 represents the impact of the CO_2 fertilization effect and climate change, and S3 represents the impact of the CO_2 fertilization effect, climate change, and LUC.

Models	Spatial resolution	S1[a]	S2	S3	References
CABLE	0.5º × 0.5º	√		√	Haverd et al., 2018
CLASS-CTEM	T42	√	√	√	Melton and Arora 2016
CLM4.5	0.94º × 1.25º	√	√	√	Oleson et al., 2010
DLEM	0.5º × 0.5º	√	√	√	Tian et al. 2015
ISAM	0.5º × 0.5º	√	√	√	Jain et al., 2013
OCN	0.5º × 0.5º			√	Zaehle and Friend 2010
ORCHIDEE-MICT	1º × 1º			√	Guimberteau et al., 2018
ORCHIDEE	0.5º × 0.5º	√	√	√	Krinner et al., 2005
VEGAS	0.5º × 0.5º	√	√	√	Zeng et al., 2005
VISIT	0.5º × 0.5º	√	√	√	Ito and Inatomi., 2011

[a]Simulation datasets in the corresponding experiments (S1, S2, and S3) as available for models indicated with the notation of "√".

2.2 FLUXCOM GPP

The FLUXCOM datasets comprised of 120 global carbon flux products generated by nine machine learning algorithms based on site-level observed GPP measured by EC associated with remote sensing information and meteorology data, but did not take the CO_2 fertilization effect into account (Jung et al., 2020). This research used the ensemble mean of GPP datasets forced by CRUJRA climate data and generated from three machine learning techniques (random forest, artificial neural network, and multivariate adaptive regression splines) from 1982 to 2015. The original spatial resolution of this dataset is 0.5 º × 0.5 º.

2.3 Satellite-based GPP products

In this study, the GLASS GPP and revised EC-LUE GPP estimates were used as representatives of long-term satellite-based GPP products from 1982 to 2015. GLASS GPP originated from the Eddy Covariance–Light Use Efficiency (EC-LUE) model (Yuan et al., 2007), which considered various impact factors (NDVI, photosynthetically activate radiation, temperature, CO_2 concentrations, the Bowen ratio of sensible to latent heat flux, water vapor pressure deficit, direct radiation fluxes, and diffuse radiation fluxes) and nine ecosystem types to accurately estimate the long-term change of GPP (Yuan et al. 2019). The original spatial resolution of this dataset is 0.05 º × 0.05 º.

The revised EC-LUE GPP is a long-term GPP dataset based on the LUE equation. Zheng et al. (2020) generated the revised EC-LUE GPP using the following formula:

$$GPP = \left(\varepsilon_{msu} \times APARsu + \varepsilon_{msh} \times APAR_{sh}\right) \times Cs \times min\left(Ts, Ws\right) \quad (1)$$

where ε_{msu} is the maximum LUE of sunlit leaves and ε_{msh} is the maximum LUE of shaded leaves; $APARsu$ is the PAR absorbed by sunlit leaves and $APAR_{sh}$ is the PAR absorbed by shaded leaves. Cs, Ts, and Ws represent the downward regulation scalars of atmospheric CO_2 concentration, temperature, and VPD on LUE with the range from 0 to 1. Specifically, the direct effect of CO_2 fertilization on GPP is determined by the following equations:

$$C_s = \frac{C_i - \varphi}{C_i + 2\varphi} \quad (2)$$

$$C_i = C_a \times \chi \quad (3)$$

where C_i represents the CO_2 concentration inside the leaf, C_a is the atmospheric CO_2 concentration, φ means the CO_2 compensation point in the absence of dark respiration (ppm), and χ means the ratio of CO_2 concentration inside the leaf to that in the atmosphere (Farquhar et al., 1980). After adding the effect of CO_2 fertilization, Zheng et al. (2020) suggested that the generated GPP was closer to the site observation data of more than five years (R^2 = 0.44) than that of other LUE models (R^2 ranged from 0.06 to 0.30). The original spatial resolution of this dataset is 0.05 º × 0.05 º.

The spatial pattern and temporal changes of the GLASS GPP and Revised EC-LUE GPP are highly consistent (Fig. S1, Fig. S2, and Fig. S3). Therefore, for simplicity, we averaged them to represent satellite-based GPP products.

2.4 NIRv dataset

删除了: Satellite-derived GPP proxy

The long-term (1982–2015) satellite growing season NIRv dataset used in this study as the GPP proxy (Badgley et al. 2019) originates from the AVHRR sensors. Following the previous study, the NIRv was first calculated as a function of monthly NDVI and near-infrared reflection of the total pixel (NIRT) via the equation of $\mathrm{NIRv} = (\mathrm{NDVI} - 0.08) \times \mathrm{NIRT}$ (Badgley et al. 2017). By defining the growing season as monthly average temperature higher than 0°C, the NIRv for each grid cell during the growing season was then aggregated into annual value. Wang et al. (2021) have shown that AVHRR NIRv could explain about 60% of the monthly variances in ground observational GPP from the FLUXNET2015 dataset, and NIRv trends could be used as the proxy of GPP trends under the different definitions of the growing season.

删除了: growing season

删除了: is

删除了: integrated yearly

2.5 Site-level GPP observations

We also adopted 20 EC sites from the FLUXNET2015 dataset (Pastorello et al., 2020) with an observation period longer than 15 years to evaluate the performance of different global GPP products. These sites, all located over Northern Hemisphere, included 5 vegetation types: evergreen broadleaf forest (EBF), evergreen needleleaf forest (ENF), deciduous broadleaf forest (DBF), grassland (GRA), and mixed forest (MF) (Table 2). The GPP variable used in this study is GPP_NT_VUT_REF. When evaluating the global gridded GPP datasets with the site observations, the bilinear interpolation method was used to interpolate the gridded data to the specific site locations.

删除了: , all distributed over Northern Hemisphere

Table 2. FLUXNET sites used in this study. The vegetation types include evergreen broadleaf forest (EBF), evergreen needleleaf forest (ENF), deciduous broadleaf forest (DBF), grassland (GRA), and mixed forest (MF).

删除了: are:

Site name	latitude	longitude	Vegetation type	Study period
FR-Pue	43.74°N	3.60°E	EBF	2000–2012
CH-Dav	46.8°N	9.85°E	ENF	1997–2014
DE-Tha	50.96°N	13.57°E	ENF	1996–2012
US-NR1	40.03°N	105.55°W	ENF	1999–2012
IT-Ren	46.59°N	11.43°E	ENF	1999–2012
NL-Loo	52.17°N	5.74°E	ENF	1996–2014
RU-Fyo	56.46°N	32.92°E	ENF	1998–2012
FI-Hyy	61.85°N	24.30°E	ENF	1996–2012
CA-Man	55.88°N	98.48°W	ENF	1994–2008
US-UMB	45.56°N	84.71°W	DBF	2000–2012
US-MMS	39.32°N	86.41°W	DBF	1999–2012
DK-Sor	55.49°N	11.64° E	DBF	2001–2012

US-Ha1	42.54°N	72.17°W	DBF	1992–2012
IT-Col	41.85°N	13.59°E	DBF	1996–2014
CA-Oas	53.63°N	106.20°W	DBF	1996–2010
US-Var	38.41°N	120.95°W	GRA	2000–2014
DK-ZaH	74.47°N	20.55° E	GRA	2000–2014
US-PFa	45.95°N	90.27°W	MF	1996–2012
BE-Bra	51.31°N	4.52°E	MF	1999–2012
BE-Vie	50.31°N	6.00°E	MF	1997–2012

2.6 Leaf area index

GLASS LAI version 05 was used to compare the TRENDY model ensemble LAI (S3) because it is an input parameter for GLASS GPP and revised EC-LUE GPP. This dataset is originated from version 4 Long-Term Data Record (LTDR) AVHRR surface reflectance product before 2001 with a spatial resolution of 0.05° × 0.05° and MODIS surface reflectance product (MOD09) after 2001 with a spatial resolution of 1km × 1km. The spatial-average method was used to aggregate the dataset to 0.05° × 0.05°. Biome-specific general regression neural networks were used to fuse these two datasets to generate a long-term LAI product (1982 - 2018), which improved performance than the original datasets. Its spatial and temporal resolutions are 0.05° × 0.05° and eight days, respectively (Xiao et al., 2016). The previous study has shown that this product performed well than other long time LAI estimation based on the evaluation of high-resolution reference maps at VAlidation of Land European Remote sensing Instruments sites (Xiao et al., 2017).

删除了:

删除了: 3

删除了: AVHRR

删除了: original

2.7 Statistical methods used

Due to the difference among spatial resolution of each product, we resampled all GPP datasets into 0.5 ° × 0.5 ° through the first-order conservative remapping method:

$$\overline{F}_k = \frac{1}{A_k}\int f\, dA \tag{4}$$

where $\overline{F}_k$ is the area-averaged destination quantity, A_k means the area of grid k, and f is the quantity in an old grid with an overlapping area with the destination grid. We resampled NIRv and LAI into 0.5 ° × 0.5 ° using bilinear interpolation and generated the annual datasets according to the weights of days. To detect the historical changes in GPP in each dataset, we calculated the global and regional total GPP and their linear trends. We also calculated the linear trends of each dataset at the pixel level to generate the spatial patterns of GPP trends. The linear trend was calculated as

$$y = kx + b + \varepsilon, \tag{5}$$

where k represents the linear trend of the time series, b is the intercept, and ε is the error term.

删除了: temporal and

删除了: We then calculated the global and regional total GPP time series from each GPP dataset and generated the linear trends of each dataset at the pixel level to generate the spatial patterns of GPP trends and at the global and zonal scales to detect the historical changes in GPP…

Finally, non-parametric Mann-Kendall trend tests were used to evaluate the level of significance for each GPP time series because it does not acquire the data to follow the normal distribution (Khaled H. Hamed, 1998).

3 Results and Discussions

3.1 Different GPP trends in DGVMs and satellite-based products

During 1982–2015, the spatial patterns of climatological annual GPP from different products are highly correlated with satellite-derived NIRv with their spatial correlation coefficients ranging from 0.84 to 0.95 (Table 3). However, the spatial distributions of the various GPP and NIRv trends are quite different. The spatial patterns of trends of NIRv, the DGVM ensemble, FLUXCOM, and satellite-based GPP during 1982–2015 are presented in Figure 1. NIRv clearly shows increasing trends in most land regions, especially in the northwest parts of Eurasia, and shows decreasing trends over Alaska and Kazakhstan (Fig. 1a). The global distribution of the DGVM ensemble GPP trends is generally consistent with satellite-derived NIRv with their spatial correlation coefficient (r) of 0.49. However, the increasing trends of the DGVM ensemble GPP in the tropical regions (Amazon and equatorial Africa) are higher than those in the boreal zone. Further, for DGVM ensemble GPP, there are about 59.8% of the global land regions showing significant positive GPP trends, and 3.8% showing significant negative GPP trends. For NIRv, 88.2% of the global land had positive GPP trends (Table 3).

删除了: 4

删除了: products

Although the DGVM ensemble GPP trends are close to those of NIRv, inconsistencies exist in spatial distribution and magnitude of GPP trends among individual model simulations. Firstly, the spatial correlations among individual models and NIRv range from 0.15 to 0.48. Secondly, the GPP simulated by the DLEM shows increasing trends in about three-fourths (77.3%) of the global land areas, while the GPP simulated by the CLASS-CTEM has increasing trends in only about one-third (33.9%) of the land area (Table 3). Finally, in magnitude, the trends of VEGAS GPP appear generally weaker than other models (Fig. S2, Fig. S4a).

删除了: than the other GPP products used here

The spatial distributions of the trends between NIRv and the remaining non-DGVM products are quite different, ranging from uncorrelated to negatively correlated (Table 3). For FLUXCOM, owing to the lack of CO_2 fertilization effect, the GPP trend pattern generally shows no significant trends over 74.1% of the land areas. And the most striking differences between NIRv and satellite-based GPP products are located in the low latitudes, especially over Amazon and Indonesia, with the latter indicating significant decreasing trends over these regions (Fig. 1d).

删除了: T

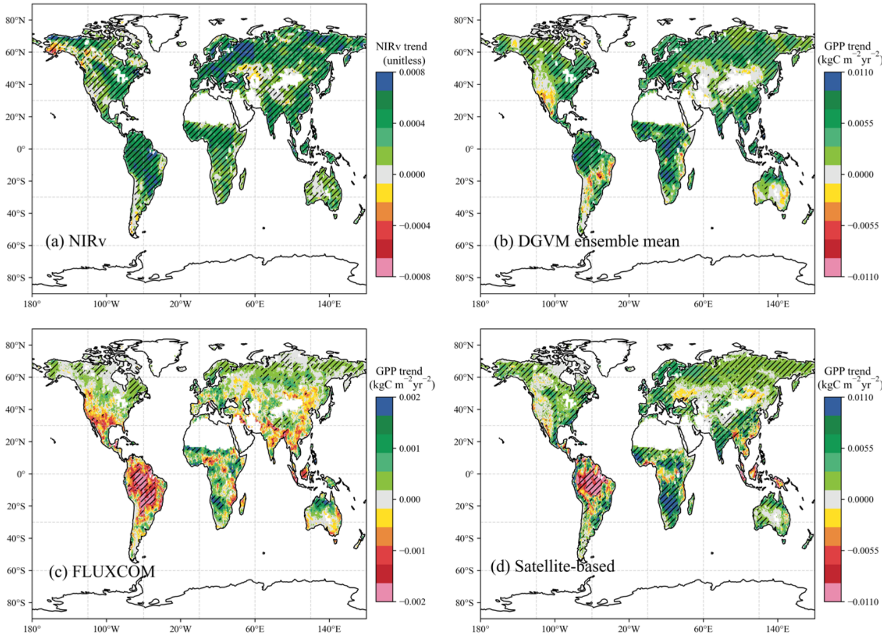

Figure 1: Geographical distributions of linear trends of NIRv and GPP during 1982–2015. (a) AVHRR NIRv, (b) Ensemble mean of TRENDY multi-model simulated GPP, (c) FLUXCOM GPP, (d) Mean of satellite-based products from revised EC-LUE and GLASS GPP. Stripped areas indicate that the trends are significant with $p < 0.05$ following the non-parametric Mann-Kendall trend test. The trends of NIRv and GPP are unitless and in kgC m^{-2} yr^{-2}, respectively. Additionally, owing to lack of the CO_2 fertilization effect in FLUXCOM GPP (c), we used a smaller scale than in (b) and (d).

删除了: is

Table 3. Spatial information for NIRv and different GPP products.

Products	Spatial correlations of climatological annual GPP with NIRv	Spatial correlations of annual GPP trends with NIRv trends	Area percentage with significant positive trends (%)	Area percentage with no significant trends (%)	Area percentage with significant negative trends (%)

DGVM ensemble mean	0.94	0.49	59.8	36.4	3.8
CABLE	0.89	0.39	56.2	41.1	2.7
CLASS-CTEM	0.90	0.38	33.9	61.3	4.8
CLM4.5	0.85	0.42	42.6	55.0	2.4
DLEM	0.84	0.44	77.3	20.4	2.3
ISAM	0.93	0.42	64.5	31.9	3.6
OCN	0.94	0.48	59.4	37.8	2.8
ORCHIDEE-MICT	0.90	0.20	52.6	41.9	5.5
ORCHIDEE	0.89	0.20	49.3	45.6	5.1
VEGAS	0.89	0.15	51.4	37.4	11.2
VISIT	0.86	0.22	51.4	42.7	5.9
GLASS	0.95	-0.01	46.4	42.6	11.0
Revised EC-LUE	0.91	-0.03	48.7	40.7	10.6
FLUXCOM	0.93	-0.26	15.1	74.4	10.5
NIRv	-	-	88.2	8.3	3.5

As mentioned above, the trends of DGVM ensemble GPP and NIRv show relatively consistent patterns for 1982–2015. However, the DGVM ensemble mean GPP shows slightly stronger trends over the tropics than over Northern Hemisphere, whereas NIRv has relatively stronger increasing trends over Northern Hemisphere (Fig. 2a). The tropical region shows the most extensive inter-model spread for the DGVM ensemble, with the strongest trends in CABLE and the weakest trends in VEGAS (Fig. S4a, Fig. S5b). The latitudinal distribution of satellite GPP products is quite different from DGVM ensemble and NIRv. Satellite-based GPP shows a significant decrease over the tropical region, rebounding to the most substantial increase located between 15°S and 25°S. The GPP increases in the middle and high latitudes of the northern hemisphere, but its magnitude is weaker than that of the DGVM ensemble in the most northern regions.

The GPP trends are quite different for the long-term (1982–2015) and recent short-term (2001–2015) periods (Fig. 2b, Fig. S4, Fig. S6). Comparing to the comparable trend magnitudes of DGVM ensemble mean GPP and NIRv over NH during these two periods, the DGVM ensemble mean GPP trends show much stronger increase but NIRv appears a little weakened increase over tropical regions during 2001–2015 (Figs. 2a and b). Additionally, satellite-based GPP products indicate a much stronger GPP decrease over the tropical regions and no noticeable trends in mid-latitudes of the Northern Hemisphere after 2000 (Fig.

删除了: **TRENDY**

删除了: There are sufficient numbers of pixels available in these regions to lend confidence to our results (Fig. 2c).

删除了: Between 2001 and 2015, t

删除了: increases more than NIRv over tropical regions and is consistent with NIRv in middle and high latitudes in the Northern Hemisphere

删除了: However

删除了: ing signal

删除了: 2001

删除了: compared to the long-term trend

2b). Also, FLUXCOM GPP trends are near zero in most latitudinal bands during these two periods (Figs. 2a and b), owing to the lack of CO_2 fertilization effect (Jung et al., 2020).

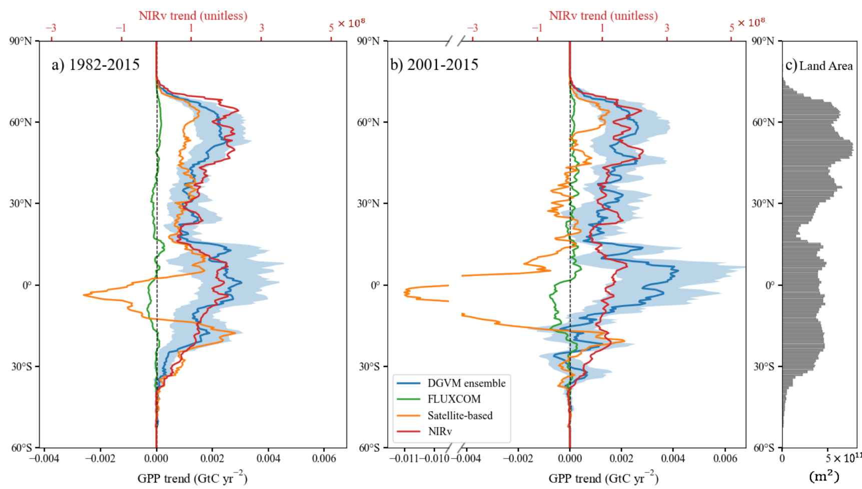

Figure 2. Latitudinal profiles of trends of annual zonal total NIRv and GPP (0.5° latitudinal bins). Results for the DGVM ensemble mean (blue), FLUXCOM GPP (green), satellite-based products (orange), and NIRv (red) during 1982–2015 (a) and 2001–2015 (b), respectively. The GPP values are given on the bottom axis and the NIRv values on the top axis. The shaded areas represent the standard deviation of the individual TRENDY model simulated GPP trend. The units of the NIRv and GPP trends are unitless and GtC yr^{-2}, respectively. (c) represents the latitudinal total vegetated land areas.

The relative changes and linear trends of annual total GPP among the DGVM simulations, FLUXCOM, and satellite-based GPP products, vary substantially both globally and regionally (Fig. 3, Fig. S3). Based on the analysis over the 34 years, the trend of global GPP was about 0.37 ± 0.08 (DGVM ensemble mean ± 95% confidence intervals), 0.0 (FLUXCOM), and 0.18 (satellite-based GPP products) GtC $year^{-2}$, respectively (Fig. 3d). Before 2001, the GPP trend of satellite-based products was generally stronger than that of DGVMs (Fig. 3a). Separating the global land into the tropics plus extra-tropical southern hemisphere (Trop+SH: 90°S–23°N) and extra-tropical northern hemisphere (NH: 23°N–90°N), results show that more than half of the increase of GPP in the DGVM ensemble is from the Trop+SH (57%). In comparison, the increase of GPP in satellite-based GPP products is mainly attributed to the NH (60%) rather than Trop+SH (40%) (Fig. 3d). In individual models, with the

删除了:

设置了格式: 下标

删除了:

删除了: change of

删除了: along the latitudes

删除了: and the linear trends of GPP

删除了: instead of

删除了: the majority of them show similar results to the model ensemble mean. …W
W

删除了: W

exception of ORCHIDEE-MICT and VEGAS, the others indicate that Trop+SH largely contributes to the global GPP trend (ranging from 54.3% to 65.3%) (Fig. 3d).

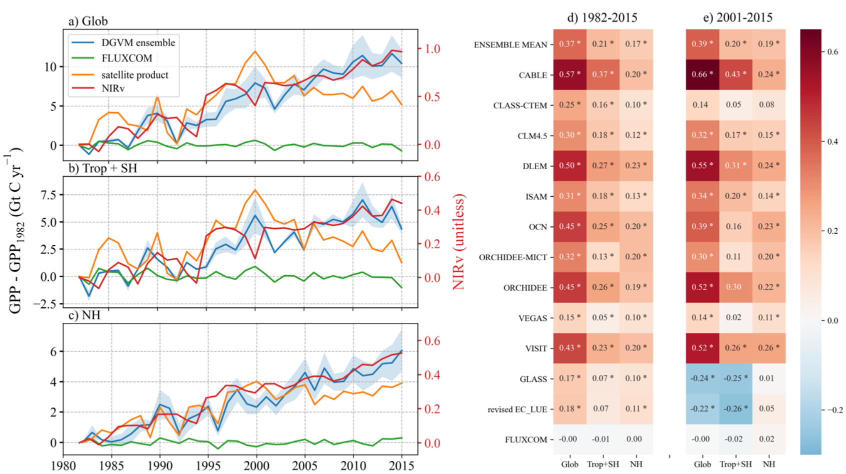

Figure 3. Linear trends of global and regional total GPP. Changes of annual total GPP relative to 1982, based on DGVM ensemble mean (blue), FLUXCOM (green) , and satellite-based products (orange), compared to AVHRR-NIRv (red), for global (a), Trop+SH (b), and NH (c). The shaded areas denote the TRENDY inter-model 1-σ spread. (d and e) Global and regional GPP trends in individual models and products for the period of 1982–2015 and 2001–2015, respectively. Asterisks indicate that the trend is significant with p < 0.05 following the non-parametric Mann-Kendall trend test.

After 2000, there were obvious differences in the trend between DGVM ensemble and satellite-based GPP products, with the satellite-based GPP products showing an obvious turning point at the year of 2000 (Figs. 3a-c), confirming the previous studies (Yuan et al., 2019; Madani et al., 2020). Both GLASS and revised EC-LUE GPP changed from significant increasing trends to significant decreasing trends, resulting mainly from Trop+SH (Figs. 3a-c). Studies based on satellite-based GPP products suggested that this transition was mainly due to the increased atmospheric vapor pressure deficit in the tropical zones (Yuan et al., 2019; Madani et al., 2020). Meanwhile, the increasing GPP trend in the NH was greatly weakened (from 0.10 to 0.01 GtC year^{-2} for GLASS and from 0.11 to 0.05 GtC year^{-2} for revised EC-LUE). In contrast, DGVM ensemble mean GPP and NIRv kept increasing. However, in detail, four out of ten DGVM models (CLASS-CTEM, OCN, ORCHIDEE-MICT, and VEGAS) simulated weakened GPP increasing signals primarily from the Trop+SH (Figs. 3d and e).

删除了: (a, b, and c)
删除了: , and FLUXCOM (green)
删除了: (the standard deviation of the annual aggregated time series)…
删除了: 2000
删除了:
删除了: 0
删除了: Hashimoto et al., 2013;
删除了: increasing
删除了: Similar to the spatial distribution, the FLUXCOM GPP has no noticeable trends in the two study periods.
删除了: ↵

In general, we found that, for the two study periods, the trends from DGVM GPP have higher consistencies with the trends of NIRv at the global and regional scales compared with satellite-based GPP. It maybe suggests that long-term trends of GPP from DGVM ensemble results have better performance than satellite-derived GPP products.

3.2 Trend attributions in DGVMs

We analyzed the contributions of three drivers (CO_2 fertilization effect, climate change, and LUC) to the GPP trends during 1982–2015 by using the results of the TRENDY sensitivity experiments (Fig. 4). Globally, DGVM ensemble results suggest that the CO_2 fertilization effect is the dominant driver to the increasing GPP (0.29 GtC year^{-2} accounting for 83.9%), followed by climate change (0.09 GtC year^{-2} accounting for 26.5%). Additionally, LUC has little effect on the trend of GPP (−0.04 GtC year^{-2} accounting for −10.4%). For individual model simulations, the contributions from CO_2 fertilization effect, climate change, and LUC range from 65.7% to 116.3%, 2% to 50.4%, and −18.4% to 5.5%, respectively. The model simulations for the period of 2001–2015 show similar results (Fig. S7).

The spatial distributions of GPP trends indicate that the CO_2 fertilization effect consistently increases global GPP, especially in tropical rainforest areas (Fig. 5a). Climate change has inhomogeneous effects on GPP owing to different regional changes of climate elements (Fig. 5c and Figs. S8a and b) associated with different vegetation sensitivities to each climate element (Wang et al., 2016; Jung et al., 2017). For instance, in the high northern latitudes, global warming dominates the increase of GPP (Fig. 5c, Fig. S8a, and Fig. S9c); the increase in temperature and decrease in precipitation over Amazon lead to the GPP decrease; the increase of GPP over Equatorial Africa appears to be consistent with the increase of the precipitation based on visual comparison against the trends for the CRU observational dataset (Fig. 5c and Fig. S8b). Concentrated in the Trop+SH, LUC basically weakens GPP (Fig. 5e and Fig. S9a), mainly due to deforestation (Friedlingstein et al., 2019).

删除了: s

删除了: to

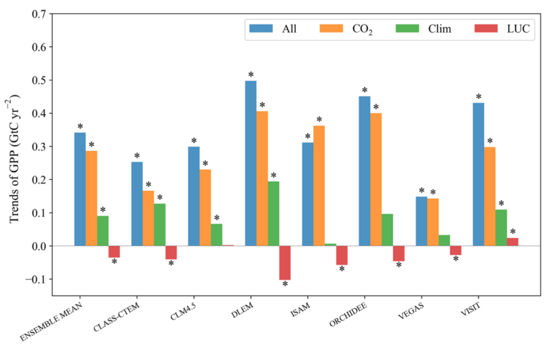

Figure 4. Attributions of global total GPP trends for TRENDYv6 simulations from 1982 to 2015: CO_2 fertilization effect (S1), climate (S2-S1), and land-use change (S3-S2). "All" gives the values of the reference simulation that includes the effect of all three drivers (S3). Asterisks indicate that the trend is significant with $p < 0.05$ following the non-parametric Mann-Kendall trend test.

3.3 Uncertainties in GPP trends

3.3.1 DGVM simulations

By analyzing the simulation results driven by each factor, it can be found that though the CO_2 fertilization effect has the most considerable contribution to the global GPP trend, it has the largest inter-model uncertainty (σ = 0.11 GtC yr^{-2}) among three drivers (Fig. 4). A previous study showed that some models might overestimate the CO_2 fertilization effect on stomatal closure (Anav et al., 2015). The spatial pattern of the standard deviation among each model indicates that the inter-model spreads are mainly located in the Trop+SH (Fig. 5h). The inter-model spread attributed to the CO_2 fertilization effect shows a consistently positive effect on GPP at the global scale (Figs. 5a and b). By contrast, the inter-model spreads driven by climate change and LUC over Trop+SH outweigh the CO_2 fertilization effect (Figs. 5b, d, and f). However, because the inhomogeneous impacts on GPP from climatic elements can offset each other to a large extent (Fig. 5c), it makes the largest inter-model uncertainty of CO_2 fertilization to the global GPP increase rather than the climate effect. Meanwhile, the largest uncertainties in the impact of LUC on GPP trends concentrate over 20º–40ºS in South America.

We further calculated the spatial correlation coefficients among the GPP trends of each model S3 simulation to quantify their spatial consistencies. The correlation coefficients in pairs among individual models varied from 0.16 to 0.61 (Fig. S10), implying that large uncertainties existed in the distribution of GPP trends among models, which were caused by differences in model structures and parameterizations (Rogers, 2014; Rogers et al., 2017). Furthermore, studies have shown that the global

删除了: ,
删除了: uncertainty
删除了: increase
删除了: s
删除了: between
删除了: each

GPP increase can be largely overestimated without nitrogen (N) constraints, especially in the tropical region, where the nitrogen limitation will reduce the photosynthetic capacity of vegetations and weaken its response to the increasing atmospheric CO_2 concentration (He et al., 2017; Terrer et al., 2019). Phosphorus (P) availability also limits the extent to which plants respond to the CO_2 fertilization effect, which is especially relevant in the Amazon forest (Fleischer et al., 2019). Therefore, DGVM ensemble GPP may overestimate the increasing GPP trend in the tropical regions since not all of the models used in this study take the effect of N limitation into consideration, and no model includes P limitation to the CO_2 fertilization effect.

删除了: will

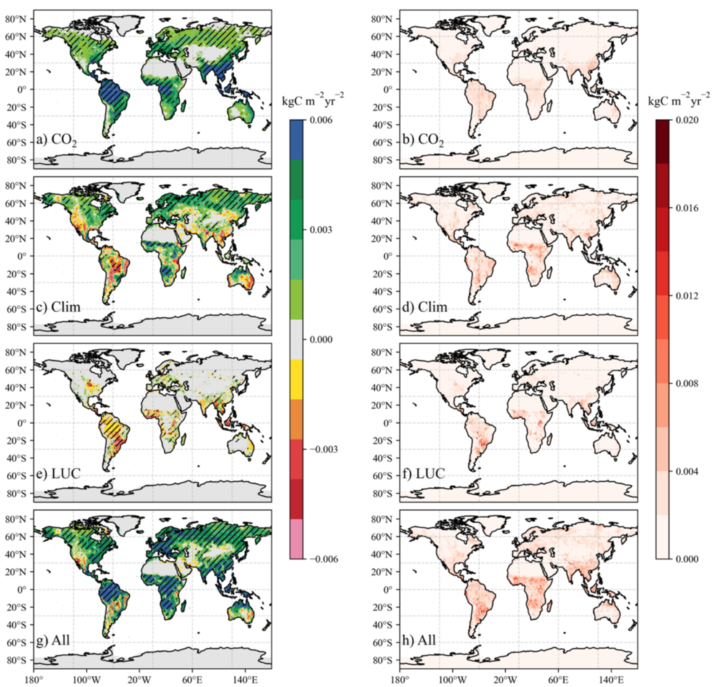

Figure 5. The spatial distribution patterns and the inter-model spreads of GPP trends from the DGVM ensemble. (a and b) GPP trends and spreads owing to CO_2 fertilization effect; (c and d) GPP trends and spreads owing to climate change; (e and f) GPP trends and spreads owing to LUC; (g and h) GPP trends and spreads from the combined effects of all drivers (S3). Stripped areas indicate that the trend is significant with $p < 0.05$ following the non-parametric Mann-Kendall trend test.

3.3.2 Satellite-based GPP products

In this study, GLASS GPP and revised EC-LUE GPP were used as a representative of long-term satellite-based GPP products. As an essential input in the LUE model (Eq. 1), APAR is a function of LAI, suggesting that LAI is a key parameter in satellite-derived GPP. The GLASS LAI product was used in calculating both the GLASS GPP and the revised EC-LUE GPP products. The spatial correlation coefficient of trends between GLASS LAI and satellite-based GPP (i.e., the mean of GLASS GPP and revised EC-LUE GPP) is 0.42. A previous study over China has shown that satellite-based LAI datasets play a more important role in GPP estimation than meteorological data for all land cover types (Liu et al., 2014). Also, the spatial distribution of trends between LAI and GPP simulated from the DGVM ensemble is even more consistent (r = 0.77), confirming the previous studies showing that the trends of GPP and LAI are highly correlated in biome models (Ito et al., 2017; Liu et al., 2019), and the changes of GPP and LAI are consistent in earth system models from CMIP5 (Hashimoto et al., 2019).

Figure 6 compares the LAI trends of GLASS and the DGVM ensemble during 2001–2015. The spatial distribution of DGVM LAI indicates significant increasing trends over the boreal forest regions, Indonesia, Equatorial Africa, and India, and significant decreasing trends over Kazakhstan, Southeast Asia, and Western Australia. The trends of GLASS LAI were obviously weaker than that of the DGVM ensemble, especially in the equatorial Africa region, northern Amazon region, Indonesia, and Northern high latitudes. The large inconsistencies between the LAI from the DGVMs and those observed in the satellite products could lead to substantial uncertainties in generating/simulating the global GPP (Fig. 1 and Fig. 6). Xiao et al. (2017) suggested that the trends of four satellite-derived LAI products showed large discrepancies in equatorial Africa from 1982 to 2011 and differed across each vegetation type. Jiang et al (2017) revealed that NOAA satellite orbit changes and MODIS sensor degradation might cause long-term satellite-derived LAI products inconsistent with each other. Xie et al. (2019) also suggested that satellite-derived LAI datasets can cause uncertainties in GPP estimations through model structure and the complexity of the terrain. Hence, the long-term trends of satellite GPP products based on satellite-derived LAI remain highly uncertain (Smith et al., 2016; Jiang et al., 2017; Liu et al., 2018).

删除了: (Xiao et al., 2017)

删除了: ,

删除了: (Xie et al., 2019)

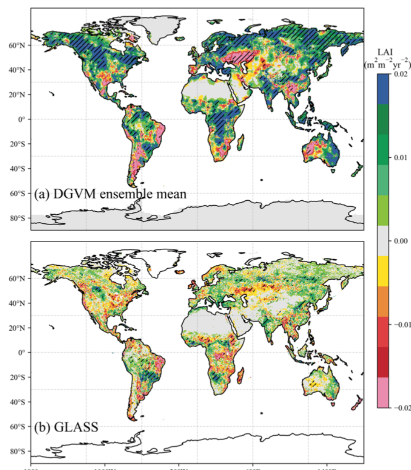

Figure 6. The spatial distributions of LAI trends ($m^2 m^{-2} yr^{-2}$) from (a) DGVM ensemble mean and (b) GLASS from 2001 to 2015. Striped areas indicate that the trend is significant with $p < 0.05$ following the non-parametric Mann-Kendall trend test.

3.3.3 Evaluations at site-level

删除了: **of**

删除了: **GPP trends**

We further adopted 20 sites with observations longer than 15 years from FLUXNET2015 datasets to evaluate long-term GPP trends from global products and simulations. Compared to the site observations, the magnitudes of GPP at most of site locations were underestimated by satellite-based GPP products, FLUXCOM, and the DGVM ensemble mean. Also, the interannual variation of GPP at sites are more obvious than those of global GPP products and NIRv (Fig. 7). This is possibly due to the fact that climate variables at 0.5-degree grid cells are smoothed out compared to those recorded at individual sites, which leads to a moderate GPP variation.

删除了: and long-term trend

More than half of the sites indicate that FLUXNET GPP has increased on a long-time scale (Fig. 7, Fig. S11), which was mainly caused by rising LUE due to the CO_2 fertilization effect and increased green vegetation cover (Cai and Prentice, 2020). Although FLUXCOM was upscaled from FLUXNET datasets, it did not capture the trends of GPP observed at sites, which was also mentioned by Anav et al. (2015). Sites with significant increasing GPP trends were all captured by DGVM ensemble mean, but some were missed by satellite-based GPP (Figs. 7b, d, k, l, m, s, and t). Furthermore, none of sites with decreasing GPP trends were reflected in the global GPP products and NIRv (Figs. 7f, h, i, j, n, q, r), which may be in part due to the different spatial representativenesses between a tower fetch and a model or satellite grid point. Therefore, the uncertainty remained when using the site-level observed GPP to evaluate the GPP trends of the DGVM simulations and satellite-based GPP products. We also selected sites with observation longer than 12 years and found similar results (Fig. S12). It is worth mentioning that sites with more than 15 years of observations were all located at NH (from 39.32°N to 50.96°N) (Table 2), and only three sites with more than 12 years of observations located at Trop+SH (Table S2).Therefore, it is hardly for us to evaluate the GPP trends of global products over the Trop+SH by using the GPP observations from sites.

删除了: .

删除了: I

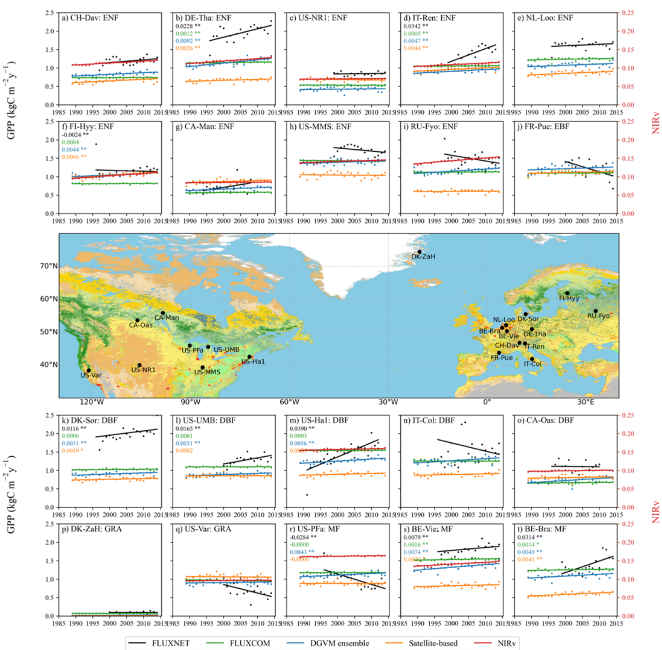

Figure 7. Comparisons of annual GPP over different FLUXNET2015 sites (black), FLUXCOM (green), satellite-based product (orange), DGVM ensemble (blue), and NIRv (red). The global GPP datasets were interpolated into the locations of these 20 sites according to the bilinear interpolation method. Observation sites with significant trends are marked with values. Single (*) and double (**) asterisks indicate that the trend is significant with $p < 0.1$ and $p < 0.05$ following the non-parametric Mann-Kendall trend test. The units of GPP and GPP trend are kgC m^{-2} yr^{-1} and kgC m^{-2} yr^{-2} respectively.

4 Conclusions

Based on five kinds of GPP or GPP-related datasets, including satellite-based products, the upscaled product from EC measurements, DGVM simulations, satellite-observed proxy (NIRv), and site-level observations, we comprehensively assessed the global and regional GPP trends during 1982−2015. The simulated spatial pattern of GPP trends from the DGVM ensemble is highly consistent with NIRv, but shows considerable inconsistency with satellite-based GPP products, especially in the tropical regions. After 2000, the GPP generated by the satellite-based GPP products decreased significantly in Trop+SH, and the increasing trend in NH also weakened. However, the results of DGVMs showed that global GPP kept increasing after 2000, even in the tropical regions, which was closer to the performance of NIRv. By analyzing the impacts of different drivers in DGVM simulations, the results indicate that the CO_2 fertilization effect has the dominant contribution to the global GPP. Spatially, the CO_2 fertilization effect makes the global GPP increased consistently, while climate has inhomogeneous impact on GPP trends over different regions.

删除了: machine learning models

删除了: 2000

删除了: 0

删除了: each driving factor

We further explored the uncertainties in GPP trends among these different datasets. For DGVM ensemble, globally, the CO_2 fertilization effect causes the largest inter-model spread. At the grid cell level, the uncertainties in simulated GPP trends concentrate over the Trop+SH, which result mainly from climate and LUC. Furthermore, the large discrepancy in the GPP trends between DGVM ensemble and satellite-based GPP products is, to a large extent, induced by the difference of vegetation canopy structure parameter (LAI). Therefore, the highly uncertain satellite-derived LAI data in the tropical regions increase the uncertainty of satellite GPP products and weaken their reliability in explaining changes in the global GPP.

Finally, GPP trends from satellite-based products and DGVM simulations were evaluated by using the FLUXNET2015 dataset. Results show that all of sites with significant increasing GPP trends can be captured by DGVM ensemble mean, but some of them were missed by satellite-based GPP. Also, none of sites with decreasing GPP trends were reflected in the global GPP products. Therefore, uncertainty remained when using the FLUXNET observed GPP to evaluate the GPP trends of the global GPP products.

删除了: And

Generally, the differences among models, observations, and products suggest the importance of the research on the GPP trend and make our caution to interpret the mechanisms of the global carbon cycle by using the long-term GPP products.

Data Availability. All data acquired or used in this analysis are available from the links in Table S1.

Author contributions. ZN, WJ, and YRQ conceived and designed this study. YRQ and TWH completed the statistical analysis and prepared figures. YRQ and WJ drafted the manuscript with contributions from all authors.

Competing interests. The authors declare that they have no conflict of interest.

Acknowledgments. We gratefully acknowledge the TRENDY DGVM community and all people and institutions who provided datasets used in this study. We thank discussion with Shengjie Zhou, Huihang Sun, Xiaohui Lin, Xing Yan, Han Mei, and Zhiqiang Liu. This work was supported by the National Key R&D Program of China (2017YFB0504000, 2020YFA0607504, and 2021YFB3901001), and the National Natural Science Foundation of China (41807434). MJM has been supported by the H2020 European Research Council (grant no. 776810).

删除了: This work was supported by the National Key R&D Program of China (No. 2017YFB0504000). Jun Wang was supported by the National Natural Science Foundation of China (41807434), National Key R&D Program of China (2020YFA0607504), and Fundamental Research Funds for the Central Universities (0904-14380028).

References

Alemohammad, S. H., Fang, B., Konings, A. G., Aires, F., Green, J. K., Kolassa, J., Miralles, D., Prigent, C., and Gentine, P.: Water, Energy, and Carbon with Artificial Neural Networks (WECANN): a statistically based estimate of global surface turbulent fluxes and gross primary productivity using solar-induced fluorescence, Biogeosciences, 14, 4101-4124, 10.5194/bg-14-4101-2017, 2017.

Anav, A., Friedlingstein, P., Beer, C., Ciais, P., Harper, A., Jones, C., Murray-Tortarolo, G., Papale, D., Parazoo, N. C., Peylin, P., Piao, S., Sitch, S., Viovy, N., Wiltshire, A., and Zhao, M.: Spatiotemporal patterns of terrestrial gross primary production: A review, Reviews of Geophysics, 53, 785-818, 10.1002/2015rg000483, 2015.

Bacour, C., Maignan, F., MacBean, N., Porcar-Castell, A., Flexas, J., Frankenberg, C., Peylin, P., Chevallier, F., Vuichard, N., and Bastrikov, V.: Improving Estimates of Gross Primary Productivity by Assimilating Solar-Induced Fluorescence Satellite Retrievals in a Terrestrial Biosphere Model Using a Process-Based SIF Model, Journal of Geophysical Research-Biogeosciences, 10.1029/2019jg005040, 2019.

Badgley, G., Field, C. B., and Berry, J. A.: Canopy near-infrared reflectance and terrestrial photosynthesis, Science Advances, 3, 10.1126/sciadv.1602244, 2017.

Badgley, G., Anderegg, L. D. L., Berry, J. A., and Field, C. B.: Terrestrial gross primary production: Using NIRV to scale from site to globe, Global Change Biology, 25, 3731-3740, 10.1111/gcb.14729, 2019.

Beer, C., Reichstein, M., Tomelleri, E., Ciais, P., Jung, M., Carvalhais, N., Rodenbeck, C., Arain, M. A., Baldocchi, D., Bonan, G. B., Bondeau, A., Cescatti, A., Lasslop, G., Lindroth, A., Lomas, M., Luyssaert, S., Margolis, H., Oleson, K. W., Roupsard, O., Veenendaal, E., Viovy, N., Williams, C., Woodward, F. I., and Papale, D.: Terrestrial gross carbon dioxide uptake: global distribution and covariation with climate, Science, 329, 834-838, 10.1126/science.1184984, 2010.

Cai, W. and Prentice, I. C.: Recent trends in gross primary production and their drivers: analysis and modelling at flux-site and global scales, Environmental Research Letters, 15, 10.1088/1748-9326/abc64e, 2020.

Camps-Valls, G., Campos-Taberner, M., Moreno-Martinez, A., Walther, S., Duveiller, G., Cescatti, A., Mahecha, M. D., Munoz-Mari, J., Javier Garcia-Haro, F., Guanter, L., Jung, M., Gamon, J. A., Reichstein, M., and Running, S. W.: A unified vegetation index for quantifying the terrestrial biosphere, Science Advances, 7, 10.1126/sciadv.abc7447, 2021.

Chen, M., Rafique, R., Asrar, G. R., Bond-Lamberty, B., Ciais, P., Zhao, F., Reyer, C. P. O., Ostberg, S., Chang, J., Ito, A., Yang, J., Zeng, N., Kalnay, E., West, T., Leng, G., Francois, L., Munhoven, G., Henrot, A., Tian, H., Pan, S., Nishina, K., Viovy, N., Morfopoulos, C., Betts, R., Schaphoff, S., Steinkamp, J., and Hickler, T.: Regional contribution to variability and trends of global gross primary productivity, Environmental Research Letters, 12, 10.1088/1748-9326/aa8978, 2017.

Farquhar, G. D., von Caemmerer, S., and Berry, J. A.: A biochemical model of photosynthetic CO2 assimilation in leaves of C 3 species, Planta, 149, 78-90, 10.1007/BF00386231, 1980.

Fleischer, K., Rammig, A., De Kauwe, M. G., Walker, A. P., Domingues, T. F., Fuchslueger, L., Garcia, S., Goll, D. S., Grandis, A., Jiang, M., Haverd, V., Hofhansl, F., Holm, J. A., Kruijt, B., Leung, F., Medlyn, B. E., Mercado, L. M., Norby, R. J., Pak, B., von Randow, C., Quesada, C. A., Schaap, K. J., Valverde-Barrantes, O. J., Wang, Y.-P., Yang, X., Zaehle, S., Zhu, Q., and Lapola, D. M.: Amazon forest response to CO2 fertilization dependent on plant phosphorus acquisition, Nature Geoscience, 12, 736-741, 10.1038/s41561-019-0404-9, 2019.

Frankenberg, C., Fisher, J. B., Worden, J., Badgley, G., Saatchi, S. S., Lee, J.-E., Toon, G. C., Butz, A., Jung, M., Kuze, A., and Yokota, T.: New global observations of the terrestrial carbon cycle from GOSAT: Patterns of plant fluorescence with gross primary productivity, Geophysical Research Letters, 38, 10.1029/2011gl048738, 2011.

Friedlingstein, P., Jones, M. W., O'Sullivan, M., Andrew, R. M., Hauck, J., Peters, G. P., Peters, W., Pongratz, J., Sitch, S., Le Quere, C., Bakker, D. C. E., Canadell, J. G., Ciais, P., Jackson, R. B., Anthoni, P., Barbero, L., Bastos, A., Bastrikov, V., Becker, M., Bopp, L., Buitenhuis, E., Chandra, N., Chevallier, F., Chini, L. P., Currie, K. I., Feely, R. A., Gehlen, M., Gilfillan, D., Gkritzalis, T., Goll, D. S., Gruber, N., Gutekunst, S., Harris, I., Haverd, V., Houghton, R. A., Hurtt, G., Ilyina, T., Jain, A. K., Joetzjer, E., Kaplan, J. O., Kato, E., Goldewijk, K. K., Korsbakken, J. I., Landschuetzer, P., Lauvset, S. K., Lefevre, N., Lenton, A., Lienert, S., Lombardozzi, D., Marland, G., McGuire, P. C., Melton, J. R., Metzl, N., Munro, D. R., Nabel, J. E. M. S., Nakaoka, S.-I., Neill, C., Omar, A. M., Ono, T., Peregon, A., Pierrot, D., Poulter, B., Rehder, G., Resplandy, L., Robertson, E., Rodenbeck, C., Seferian, R., Schwinger, J., Smith, N., Tans, P. P., Tian, H., Tilbrook, B., Tubiello, F. N., van der Werf, G. R., Wiltshire, A. J., and Zaehle, S.: Global Carbon Budget 2019, Earth System Science Data, 11, 1783-1838, 10.5194/essd-11-1783-2019, 2019.

Guanter, L., Zhang, Y., Jung, M., Joiner, J., Voigt, M., Berry, J. A., Frankenberg, C., Huete, A. R., Zarco-Tejada, P., Lee, J.-E., Moran, M. S., Ponce-Campos, G., Beer, C., Camps-Valls, G., Buchmann, N., Gianelle, D., Klumpp, K., Cescatti, A., Baker, J. M., and Griffis, T. J.: Global and time-resolved monitoring of crop photosynthesis with chlorophyll fluorescence, Proceedings of the National Academy of Sciences of the United States of America, 111, E1327-E1333, 10.1073/pnas.1320008111, 2014.

Guimberteau, M., Zhu, D., Maignan, F., Huang, Y., Yue, C., Dantec-Nedelec, S., Ottle, C., Jornet-Puig, A., Bastos, A., Laurent, P., Goll, D., Bowring, S., Chang, J., Guenet, B., Tifafi, M., Peng, S., Krinner, G., Ducharne, A., Wang, F., Wang, T., Wang, X., Wang, Y., Yin, Z., Lauerwald, R., Joetzjer, E., Qiu, C., Kim, H., and Ciais, P.: ORCHIDEE-MICT (v8.4.1), a land surface model for the high latitudes: model description and validation, Geoscientific Model Development, 11, 121-163, 10.5194/gmd-11-121-2018, 2018.

删除了:

Hashimoto, H., Wang, W., Milesi, C., Xiong, J., Ganguly, S., Zhu, Z., and Nemani, R.: Structural Uncertainty in Model-Simulated Trends of Global Gross Primary Production, Remote Sensing, 5, 1258-1273, 10.3390/rs5031258, 2013.

Hashimoto, H., Nemani, R., Bala, G., Cao, L., Michaelis, A., Ganguly, S., Wang, W., Milesi, C., Eastman, R., Lee, T., and Myneni, R.: Constraints to Vegetation Growth Reduced by Region-Specific Changes in Seasonal Climate, Climate, 7, 10.3390/cli7020027, 2019.

Haverd, V., Smith, B., Nieradzik, L., Briggs, P. R., Woodgate, W., Trudinger, C. M., Canadell, J. G., and Cuntz, M.: A new version of the CABLE land surface model (Subversion revision r4601) incorporating land use and land cover change, woody vegetation demography, and a novel optimisation-based approach to plant coordination of photosynthesis, Geoscientific Model Development, 11, 2995-3026, 10.5194/gmd-11-2995-2018, 2018.

He, L., Chen, J. M., Croft, H., Gonsamo, A., Luo, X., Liu, J., Zheng, T., Liu, R., and Liu, Y.: Nitrogen Availability Dampens the Positive Impacts of CO2Fertilization on Terrestrial Ecosystem Carbon and Water Cycles, Geophysical Research Letters, 44, 11,590-511,600, 10.1002/2017gl075981, 2017.

Huete, A., Didan, K., Miura, T., Rodriguez, E. P., Gao, X., and Ferreira, L. G.: Overview of the radiometric and biophysical performance of the MODIS vegetation indices, Remote Sensing of Environment, 83, 195-213, 10.1016/s0034-4257(02)00096-2, 2002.

Huntzinger, D. N., Schwalm, C., Michalak, A. M., Schaefer, K., King, A. W., Wei, Y., Jacobson, A., Liu, S., Cook, R. B., Post, W. M., Berthier, G., Hayes, D., Huang, M., Ito, A., Lei, H., Lu, C., Mao, J., Peng, C. H., Peng, S., Poulter, B., Riccuito, D., Shi, X., Tian, H., Wang, W., Zeng, N., Zhao, F., and Zhu, Q.: The North American Carbon Program Multi-Scale Synthesis and Terrestrial Model Intercomparison Project – Part 1: Overview and experimental design, Geoscientific Model Development, 6, 2121-2133, 10.5194/gmd-6-2121-2013, 2013.

Ito, A., Nishina, K., Reyer, C. P. O., François, L., Henrot, A.-J., Munhoven, G., Jacquemin, I., Tian, H., Yang, J., Pan, S., Morfopoulos, C., Betts, R., Hickler, T., Steinkamp, J., Ostberg, S., Schaphoff, S., Ciais, P., Chang, J., Rafique, R., Zeng, N., and Zhao, F.: Photosynthetic productivity and its efficiencies in ISIMIP2a biome models: benchmarking for impact assessment studies, Environmental Research Letters, 12, 10.1088/1748-9326/aa7a19, 2017.

Jain, A. K., Meiyappan, P., Song, Y., and House, J. I.: CO2 emissions from land-use change affected more by nitrogen cycle, than by the choice of land-cover data, Global Change Biology, 19, 2893-2906, 10.1111/gcb.12207, 2013.

Jia, B., Luo, X., Cai, X., Jain, A., Huntzinger, D. N., Xie, Z., Zeng, N., Mao, J., Shi, X., Ito, A., Wei, Y., Tian, H., Poulter, B., Hayes, D., and Schaefer, K.: Impacts of land use change and elevated CO₂ on the interannual variations and seasonal cycles of gross primary productivity in China, Earth System Dynamics, 11, 235-249, 10.5194/esd-11-235-2020, 2020.

Jiang, C., Ryu, Y., Fang, H., Myneni, R., Claverie, M., and Zhu, Z.: Inconsistencies of interannual variability and trends in long-term satellite leaf area index products, Global Change Biology, 23, 4133-4146, 10.1111/gcb.13787, 2017.

Joiner, J., Yoshida, Y., Zhang, Y., Duveiller, G., Jung, M., Lyapustin, A., Wang, Y., and Tucker, C.: Estimation of Terrestrial Global Gross Primary Production (GPP) with Satellite Data-Driven Models and Eddy Covariance Flux Data, Remote Sensing, 10, 10.3390/rs10091346, 2018.

Jung, M., Reichstein, M., Schwalm, C. R., Huntingford, C., Sitch, S., Ahlstrom, A., Arneth, A., Camps-Valls, G., Ciais, P., Friedlingstein, P., Gans, F., Ichii, K., Ain, A. K. J., Kato, E., Papale, D., Poulter, B., Raduly, B., Rodenbeck, C., Tramontana, G., Viovy, N., Wang, Y.-P., Weber, U., Zaehle, S., and Zeng, N.: Compensatory water effects link yearly global land CO2 sink changes to temperature, Nature, 541, 516-520, 10.1038/nature20780, 2017.

Jung, M., Schwalm, C., Migliavacca, M., Walther, S., Camps-Valls, G., Koirala, S., Anthoni, P., Besnard, S., Bodesheim, P., Carvalhais, N., Chevallier, F., Gans, F., Goll, D. S., Haverd, V., Köhler, P., Ichii, K., Jain, A. K., Liu, J., Lombardozzi, D., Nabel, J. E. M. S., Nelson, J. A., O'Sullivan, M., Pallandt, M., Papale, D., Peters, W., Pongratz, J., Rödenbeck, C., Sitch, S., Tramontana, G., Walker, A., Weber, U., and Reichstein, M.: Scaling carbon fluxes from eddy covariance sites to globe: synthesis and evaluation of the FLUXCOM approach, Biogeosciences, 17, 1343-1365, 10.5194/bg-17-1343-2020, 2020.

Kato, E., Kinoshita, T., Ito, A., Kawamiya, M., and Yamagata, Y.: Evaluation of spatially explicit emission scenario of land-use change and biomass burning using a process-based biogeochemical model, Journal of Land Use Science, 8, 104-122, 10.1080/1747423x.2011.628705, 2013.

Khaled H. Hamed, A. R. R.: A modified Mann-Kendall trend test for autocorrelated data, Journal of Hydrology, 14, 10.1016/S0022-1694(97)00125-X, 1998.

Krinner, G., Viovy, N., de Noblet-Ducoudre, N., Ogee, J., Polcher, J., Friedlingstein, P., Ciais, P., Sitch, S., and Prentice, I. C.: A dynamic global vegetation model for studies of the coupled atmosphere-biosphere system, Global Biogeochemical Cycles, 19, 10.1029/2003gb002199, 2005.

Liu, Y., Xue, Y., MacDonald, G., Cox, P., and Zhang, Z.: Global vegetation variability and its response to elevated CO₂, global warming, and climate variability – a study using the offline SSiB4/TRIFFID model and satellite data, Earth System Dynamics, 10, 9-29, 10.5194/esd-10-9-2019, 2019.

Liu, Y., Xiao, J., Ju, W., Zhu, G., Wu, X., Fan, W., Li, D., and Zhou, Y.: Satellite-derived LAI products exhibit large discrepancies and can lead to substantial uncertainty in simulated carbon and water fluxes, Remote Sensing of Environment, 206, 174-188, 10.1016/j.rse.2017.12.024, 2018.

Liu, Z., Shao, Q., and Liu, J.: The Performances of MODIS-GPP and -ET Products in China and Their Sensitivity to Input Data (FPAR/LAI), Remote Sensing, 7, 135-152, 10.3390/rs70100135, 2014.

MacBean, N., Maignan, F., Bacour, C., Lewis, P., Peylin, P., Guanter, L., Kohler, P., Gomez-Dans, J., and Disney, M.: Strong constraint on modelled global carbon uptake using solar-induced chlorophyll fluorescence data (vol 8, 1973, 2018), Scientific Reports, 8, 10.1038/s41598-018-28697-z, 2018.

Madani, N., Parazoo, N. C., Kimball, J. S., Ballantyne, A. P., Reichle, R. H., Maneta, M., Saatchi, S., Palmer, P. I., Liu, Z., and Tagesson, T.: Recent Amplified Global Gross Primary Productivity Due to Temperature Increase Is Offset by Reduced Productivity Due to Water Constraints, AGU Advances, 1, 10.1029/2020av000180, 2020.

Melton, J. R. and Arora, V. K.: Competition between plant functional types in the Canadian Terrestrial Ecosystem Model (CTEM) v.2.0, Geoscientific Model Development, 9, 323-361, 10.5194/gmd-9-323-2016, 2016.

Mohammed, G. H., Colombo, R., Middleton, E. M., Rascher, U., van der Tol, C., Nedbal, L., Goulas, Y., Perez-Priego, O., Damm, A., Meroni, M., Joiner, J., Cogliati, S., Verhoef, W., Malenovsky, Z., Gastellu-Etchegorry, J.-P., Miller, J. R., Guanter, L., Moreno, J., Moya, I., Berry, J. A., Frankenberg, C., and Zarco-Tejada, P. J.: Remote sensing of solar-induced chlorophyll fluorescence (SIF) in vegetation: 50 years of progress, Remote Sensing of Environment, 231, 10.1016/j.rse.2019.04.030, 2019.

Norton, A. J., Rayner, P. J., Koffi, E. N., Scholze, M., Silver, J. D., and Wang, Y.-P.: Estimating global gross primary productivity using chlorophyll fluorescence and a data assimilation system with the BETHY-SCOPE model, Biogeosciences, 16, 3069-3093, 10.5194/bg-16-3069-2019, 2019.

O'Sullivan, M., Smith, W. K., Sitch, S., Friedlingstein, P., Arora, V. K., Haverd, V., Jain, A. K., Kato, E., Kautz, M., Lombardozzi, D., Nabel, J., Tian, H., Vuichard, N., Wiltshire, A., Zhu, D., and Buermann, W.: Climate-Driven Variability and Trends in Plant Productivity Over Recent Decades Based on Three Global Products, Global Biogeochem Cycles, 34, e2020GB006613, 10.1029/2020GB006613, 2020.

Oleson, K. W., Lawrence, D. M., Gordon, B., Flanner, M. G., Kluzek, E., Peter, J., Levis, S., Swenson, S. C., Thornton, E., and Feddema, J.: Technical description of version 4.0 of the Community Land Model (CLM), 2010.

Pastorello, G., Trotta, C., Canfora, E., Chu, H., Christianson, D., Cheah, Y.-W., Poindexter, C., Chen, J., Elbashandy, A., Humphrey, M., Isaac, P., Polidori, D., Ribeca, A., van Ingen, C., Zhang, L., Amiro, B., Ammann, C., Arain, M. A., Ardo, J., Arkebauer, T., Arndt, S. K., Arriga, N., Aubinet, M., Aurela, M., Baldocchi, D., Barr, A., Beamesderfer, E., Marchesini, L. B., Bergeron, O., Beringer, J., Bernhofer, C., Berveiller, D., Billesbach, D., Black, T. A., Blanken, P. D., Bohrer, G., Boike, J., Bolstad, P. V., Bonal, D., Bonnefond, J.-M., Bowling, D. R., Bracho, R., Brodeur, J., Bruemmer, C., Buchmann, N., Burban, B., Burns, S. P., Buysse, P., Cale, P., Cavagna, M., Cellier, P., Chen, S., Chini, I., Christensen, T. R., Cleverly, J., Collalti, A., Consalvo, C., Cook, B. D., Cook, D., Coursolle, C., Cremonese, E., Curtis, P. S., D'Andrea, E., da Rocha, H., Dai, X., Davis, K. J., De Cinti, B., de Grandcourt, A., De Ligne, A., De Oliveira, R. C., Delpierre, N., Desai, A. R., Di Bella, C. M., di Tommasi, P., Dolman, H., Domingo, F., Dong, G., Dore, S., Duce, P., Dufrene, E., Dunn, A., Dusek, J., Eamus, D., Eichelmann, U., ElKhidir, H. A. M., Eugster, W., Ewenz, C. M., Ewers, B., Famulari, D., Fares, S., Feigenwinter, I., Feitz, A., Fensholt, R., Filippa, G., Fischer, M., Frank, J., Galvagno, M., Gharun, M., Gianelle, D., Gielen, B., Gioli, B., Gitelson, A., Goded, I., Goeckede, M., Goldstein, A. H., Gough, C. M., Goulden, M. L., Graf, A., Griebel, A., Gruening, C., Gruenwald, T., Hammerle, A., Han, S., Han, X., Hansen, B. U., Hanson, C., Hatakka, J., He, Y., Hehn, M., Heinesch, B., Hinko-Najera, N., Hoertnagl, L., Hutley, L., Ibrom, A., Ikawa, H., Jackowicz-Korczynski, M., Janous, D., Jans, W., Jassal, R., Jiang, S., Kato, T., Khomik, M., Klatt, J., Knohl, A., Knox, S., Kobayashi, H., Koerber, G., Kolle, O., Kosugi, Y., Kotani, A., Kowalski, A., Kruijt, B., Kurbatova, J., Kutsch, W. L., Kwon, H., Launiainen, S., Laurila, T., Law, B., Leuning, R., Li, Y., Liddell, M., Limousin, J.-M., Lion, M., Liska, A. J., Lohila, A., Lopez-Ballesteros, A., Lopez-Blanco, E., Loubet, B., Loustau, D., Lucas-Moffat, A., Lueers, J., Ma, S., Macfarlane, C., Magliulo, V., Maier, R., Mammarella, I., Manca, G., Marcolla, B., Margolis, H. A., Marras, S., Massman, W., Mastepanov, M., Matamala, R., Matthes, J. H., Mazzenga, F., McCaughey, H., McHugh, I., McMillan, A. M. S., Merbold, L., Meyer, W., Meyers, T., Miller, S. D., Minerbi, S., Moderow, U., Monson, R. K., Montagnani, L., Moore, C. E., Moors, E., Moreaux, V., Moureaux, C., Munger, J. W., Nakai, T., Neirynck, J., Nesic, Z., Nicolini, G., Noormets, A., Northwood, M., Nosetto, M., Nouvellon, Y., Novick, K., Oechel, W., Olesen, J. E., Ourcival, J.-M., Papuga, S. A., Parmentier, F.-J., Paul-Limoges, E., Pavelka, M., Peichl, M., Pendall, E., Phillips, R. P., Pilegaard, K., Pirk, N., Posse, G., Powell, T., Prasse, H., Prober, S. M., Rambal, S., Rannik, U., Raz-Yaseef, N., Reed, D., de Dios, V. R., Restrepo-Coupe, N., Reverter, B. R., Roland, M., Sabbatini, S., Sachs, T., Saleska, S. R., Sanchez-Canete, E. P., Sanchez-Mejia, Z. M., Schmid, H. P., Schmidt, M., Schneider, K., Schrader, F., Schroder, I., Scott, R. L., Sedlak, P., Serrano-Ortiz, P., Shao, C., Shi, P., Shironya, I., Siebicke, L., Sigut, L., Silberstein, R., Sirca, C., Spano, D., Steinbrecher, R., Stevens, R. M., Sturtevant, C., Suyker, A., Tagesson, T., Takanashi, S., Tang, Y., Tapper, N., Thom, J., Tiedemann, F., Tomassucci, M., Tuovinen, J.-P., Urbanski, S., Valentini, R., van der Molen, M., van Gorsel, E., van Huissteden, K., Varlagin, A., Verfaillie, J., Vesala, T., Vincke, C., Vitale, D., Vygodskaya, N., Walker, J. P., Walter-Shea, E., Wang, H., Weber, R., Westermann, S., Wille, C., Wofsy, S., Wohlfahrt, G., Wolf, S., Woodgate, W., Li, Y., Zampedri, R., Zhang, J., Zhou, G., Zona, D., Agarwal, D., Biraud, S., Torn, M., and Papale, D.: The FLUXNET2015 dataset and the ONEFlux processing pipeline for eddy covariance data, Scientific Data, 7, 10.1038/s41597-020-0534-3, 2020.

Piao, S., Wang, X., Park, T., Chen, C., Lian, X., He, Y., Bjerke, J. W., Chen, A., Ciais, P., Tommervik, H., Nemani, R. R., and Myneni, R. B.: Characteristics, drivers and feedbacks of global greening, Nature Reviews Earth & Environment, 1, 14-27, 10.1038/s43017-019-0001-x, 2020.

Rogers, A.: The use and misuse of Vc,max in Earth System Models, Photosynthesis Research, 119, 15-29, 10.1007/s11120-013-9818-1, 2014.

Rogers, A., Medlyn, B. E., Dukes, J. S., Bonan, G., von Caemmerer, S., Dietze, M. C., Kattge, J., Leakey, A. D. B., Mercado, L. M., Niinemets, U., Prentice, I. C., Serbin, S. P., Sitch, S., Way, D. A., and Zaehle, S.: A roadmap for improving the representation of photosynthesis in Earth system models, New Phytologist, 213, 22-42, 10.1111/nph.14283, 2017.

Running, S. W., Nemani, R. R., Heinsch, F. A., Zhao, M. S., Reeves, M., and Hashimoto, H.: A continuous satellite-derived measure of global terrestrial primary production, Bioscience, 54, 547-560, 10.1641/0006-3568(2004)054[0547:Acsmog]2.0.Co;2, 2004.

Ryu, Y., Berry, J. A., and Baldocchi, D. D.: What is global photosynthesis? History, uncertainties and opportunities, Remote Sensing of Environment, 223, 95-114, 10.1016/j.rse.2019.01.016, 2019.

Sitch, S., Friedlingstein, P., Gruber, N., Jones, S. D., Murray-Tortarolo, G., Ahlström, A., Doney, S. C., Graven, H., Heinze, C., Huntingford, C., Levis, S., Levy, P. E., Lomas, M., Poulter, B., Viovy, N., Zaehle, S., Zeng, N., Arneth, A., Bonan, G., Bopp, L., Canadell, J. G., Chevallier, F., Ciais, P., Ellis, R., Gloor, M., Peylin, P., Piao, S. L., Le Quéré, C., Smith, B., Zhu, Z., and Myneni, R.: Recent trends and drivers of regional sources and sinks of carbon dioxide, Biogeosciences, 12, 653-679, 10.5194/bg-12-653-2015, 2015.

Smith, W. K., Reed, S. C., Cleveland, C. C., Ballantyne, A. P., Anderegg, W. R. L., Wieder, W. R., Liu, Y. Y., and Running, S. W.: Large divergence of satellite and Earth system model estimates of global terrestrial CO2 fertilization, Nature Climate Change, 6, 306-310, 10.1038/nclimate2879, 2016.

Terrer, C., Jackson, R. B., Prentice, I. C., Keenan, T. F., Kaiser, C., Vicca, S., Fisher, J. B., Reich, P. B., Stocker, B. D., Hungate, B. A., Peñuelas, J., McCallum, I., Soudzilovskaia, N. A., Cernusak, L. A., Talhelm, A. F., Van Sundert, K., Piao, S., Newton, P. C. D., Hovenden, M. J., Blumenthal, D. M., Liu, Y. Y., Müller, C., Winter, K., Field, C. B., Viechtbauer, W., Van Lissa, C. J., Hoosbeek, M. R., Watanabe, M., Koike, T., Leshyk, V. O., Polley, H. W., and Franklin, O.: Nitrogen and phosphorus constrain the CO2 fertilization of global plant biomass, Nature Climate Change, 9, 684-689, 10.1038/s41558-019-0545-2, 2019.

Tian, H., Chen, G., Lu, C., Xu, X., Hayes, D. J., Ren, W., Pan, S., Huntzinger, D. N., and Wofsy, S. C.: North American terrestrial CO2 uptake largely offset by CH4 and N2O emissions: toward a full accounting of the greenhouse gas budget, Climatic Change, 129, 413-426, 10.1007/s10584-014-1072-9, 2015.

Wang, M.,Wang J.,Cai Q., Zeng N., Lu X.,Yang R.,Jiang F.,Wang H., and Ju W.: Considerable uncertainties in simulating land carbon sinks induced by different precipitation products, Journal of Geophysical Research: Biogeosciences, 126: e2021JG006524, 2021.

Wang, J., Zeng, N., and Wang, M.: Interannual variability of the atmospheric CO2 growth rate: roles of precipitation and temperature, Biogeosciences, 13, 2339-2352, 10.5194/bg-13-2339-2016, 2016.

Wang, J., Jiang, F., Wang, H., Qiu, B., Wu, M., He, W., Ju, W., Zhang, Y., Chen, J. M., and Zhou, Y.: Constraining global terrestrial gross primary productivity in a global carbon assimilation system with OCO-2 chlorophyll fluorescence data, Agricultural and Forest Meteorology, 304, 10.1016/j.agrformet.2021.108424, 2021a.

Wang, J., Wang, M., Kim, J.-S., Joiner, J., Zeng, N., Jiang, F., Wang, H., He, W., Wu, M., Chen, T., Ju, W., and Chen, J. M.: Modulation of Land Photosynthesis by the Indian Ocean Dipole: Satellite-Based Observations and CMIP6 Future Projections, Earths Future, 9, 10.1029/2020ef001942, 2021b.

Wang, J., Dong, J., Liu, J., Huang, M., Li, G., Running, S. W., Smith, W. K., Harris, W., Saigusa, N., Kondo, H., Liu, Y., Hirano, T., and Xiao, X.: Comparison of Gross Primary Productivity Derived from GIMMS NDVI3g, GIMMS, and MODIS in Southeast Asia, Remote Sensing, 6, 2108-2133, 10.3390/rs6032108, 2014.

Wang, S., Zhang, Y., Ju, W., Chen, J. M., Ciais, P., Cescatti, A., Sardans, J., Janssens, I. A., Wu, M., Berry, J. A., Campbell, E., Fernandez-Martinez, M., Alkama, R., Sitch, S., Friedlingstein, P., Smith, W. K., Yuan, W., He, W., Lombardozzi, D., Kautz, M., Zhu, D., Lienert, S., Kato, E., Poulter, B., Sanders, T. G. M., Kruger, I., Wang, R., Zeng, N., Tian, H., Vuichard, N., Jain, A. K., Wiltshire, A., Haverd, V., Goll, D. S., and Penuelas, J.: Recent global decline of CO2 fertilization effects on vegetation photosynthesis (vol 370, pg 1295, 2020), Science, 371, 10.1126/science.abg8637, 2021

Xiao, Z., Liang, S., and Jiang, B.: Evaluation of four long time-series global leaf area index products, Agricultural and Forest Meteorology, 246, 218-230, 10.1016/j.agrformet.2017.06.016, 2017.

删除了: c

Xie, X., Li, A., Jin, H., Tan, J., Wang, C., Lei, G., Zhang, Z., Bian, J., and Nan, X.: Assessment of five satellite-derived LAI datasets for GPP estimations through ecosystem models, Sci Total Environ, 690, 1120-1130, 10.1016/j.scitotenv.2019.06.516, 2019.

Yuan, W., Liu, S., Yu, G., Bonnefond, J.-M., Chen, J., Davis, K., Desai, A. R., Goldstein, A. H., Gianelle, D., Rossi, F., Suyker, A. E., and Verma, S. B.: Global estimates of evapotranspiration and gross primary production based on MODIS and global meteorology data, Remote Sensing of Environment, 114, 1416-1431, 10.1016/j.rse.2010.01.022, 2010.

Yuan, W., Liu, S., Zhou, G., Zhou, G., Tieszen, L. L., Baldocchi, D., Bernhofer, C., Gholz, H., Goldstein, A. H., Goulden, M. L., Hollinger, D. Y., Hu, Y., Law, B. E., Stoy, P. C., Vesala, T., Wofsy, S. C., and AmeriFlux, C.: Deriving a light use efficiency model from eddy covariance flux data for predicting daily gross primary production across biomes, Agricultural and Forest Meteorology, 143, 189-207, 10.1016/j.agrformet.2006.12.001, 2007.

Yuan, W., Zheng, Y., Piao, S., Ciais, P., Lombardozzi, D., Wang, Y., Ryu, Y., Chen, G., Dong, W., Hu, Z., Jain, A. K., Jiang, C., Kato, E., Li, S., Lienert, S., Liu, S., Nabel, J. E. M. S., Qin, Z., Quine, T., Sitch, S., Smith, W. K., Wang, F., Wu, C., Xiao, Z., and Yang, S.: Increased atmospheric vapor pressure deficit reduces global vegetation growth, Science Advances, 5, 10.1126/sciadv.aax1396, 2019.

Zaehle, S., Friend, A. D., Friedlingstein, P., Dentener, F., Peylin, P., and Schulz, M.: Carbon and nitrogen cycle dynamics in the O-CN land surface model: 2. Role of the nitrogen cycle in the historical terrestrial carbon balance, Global Biogeochemical Cycles, 24, 10.1029/2009gb003522, 2010.

Zeng, N., Mariotti, A., and Wetzel, P.: Terrestrial mechanisms of interannual CO2 variability, Global Biogeochemical Cycles, 19, 10.1029/2004gb002273, 2005.

Zhang, Y. and Ye, A.: Would the obtainable gross primary productivity (GPP) products stand up? A critical assessment of 45 global GPP products, The Science of the total environment, 783, 146965-146965, 10.1016/j.scitotenv.2021.146965, 2021.

Zheng, Y., Shen, R., Wang, Y., Li, X., Liu, S., Liang, S., Chen, J. M., Ju, W., Zhang, L., and Yuan, W.: Improved estimate of global gross primary production for reproducing its long-term variation, 1982-2017, Earth System Science Data, 12, 2725-2746, 10.5194/essd-12-2725-2020, 2020.